Investigation of the Effect of Copper-Palladium Electrocatalysts on Nitrate Reduction

by
Arthur Finstad

A THESIS

submitted to

Oregon State University

Honors College

in partial fulfillment of
the requirements for the
degree of

Honors Baccalaureate of Science in Bioengineering and Chemistry
(Honors Scholar)

Presented May 25, 2021
Commencement June 2021

AN ABSTRACT OF THE THESIS OF

Arthur Finstad for the degree of Honors Baccalaureate of Science in Bioengineering and Chemistry presented on May 25, 2021. Title: Investigation of the Effect of Copper-Palladium Electrocatalysts on Nitrate Reduction.

Abstract approved:_____

Kelsey Stoerzinger

Nitrate (NO_3^-) accumulation in water sources is a serious health and environmental concern. Common methods used to reduce NO_3^- accumulation have one or more undesirable traits that limit their efficacy in large-scale decontamination. However, treatment of NO_3^- electrochemically is a promising area of study because of the absence of toxic byproducts and potential to be performed at a low energy cost. Noble and coinage metals show varying capabilities in catalyzing the complete nitrate reduction reaction (NO_3RR), and so research has focused on bimetallic electrocatalysts that combine desirable characteristics of two metals in NO_3RR. Of the possible combinations, Cu-Pd electrocatalysts display the highest activity and selectivity for NO_3RR and are the subject of this study. Five $Cu_{100-x}Pd_x$ electrocatalysts were synthesized by electrodeposition onto FTO glass substrates, and their activity for NO_3RR was investigated using electrochemical techniques. The pure Cu electrocatalyst displayed the highest activity and best charge transfer kinetics of the set, and incorporation of Pd led to a decrease in activity and efficiency for NO_3RR. Further testing is required to ascertain the selectivity of the electrocatalysts to the preferred N_2 final product, which is a critical aspect in the electrochemical treatment of NO_3^-.

Key Words: Nitrate reduction, Electrocatalysts, Copper-Palladium

Corresponding e-mail address: finstaar@oregonstate.edu

Investigation of the Effect of Copper-Palladium Electrocatalysts on Nitrate Reduction

by
Arthur Finstad

A THESIS

submitted to

Oregon State University

Honors College

in partial fulfillment of
the requirements for the
degree of

Honors Baccalaureate of Science in Bioengineering and Chemistry
(Honors Scholar)

Presented May 25, 2021
Commencement June 2021

Honors Baccalaureate of Science in Bioengineering and Chemistry project of Arthur Finstad presented on May 25, 2021.

APPROVED:

_____

Kelsey Stoerzinger, Mentor, representing Chemical Engineering

_____

Zhenxing Feng, Committee Member, representing Chemical Engineering

_____

Tyler Radniecki, Committee Member, representing Environmental Engineering

_____

Toni Doolen, Dean, Oregon State University Honors College

I understand that my project will become part of the permanent collection of Oregon State University, Honors College. My signature below authorizes release of my project to any reader upon request.

_____

Arthur Finstad, Author

Introduction

Nitrogen is an element critical to developing and sustaining life. Atmospheric dinitrogen gas (N_2) is biologically fixed by bacteria in soil as nutrients which can then be absorbed by plants. Industrially, nitrogen is fixed in the Haber-Bosch process to create ammonia (NH_3) for fertilizer. Excess fertilizer amendment results in plants and nitrifying bacteria oxidizing NH_3 into nitrate (NO_3^-), a toxic groundwater pollutant. Partially-oxidized nitrogen gasses (NO_x) also provide a source of NO_3^- as they precipitate in the form of acid rain.[1] Anthropogenic misbalances in the nitrogen cycle have caused NO_3^- to become a leading source of groundwater contamination, which can lead to serious health and environmental consequences.[2] Current primary NO_3^- treatment methods – biological, ion exchange, and reverse osmosis – present drawbacks as space or energy intensive, and generate some form of hazardous waste, limiting scalability. Alternatively, the NO_3^- reduction reaction (NO_3RR) can be performed electrochemically, harnessing "green" electrons from renewable sources, having a broader range of scalability than conventional treatment technologies, and producing no secondary waste.[3]

The complexity of NO_3RR pathway in acidic electrolyte is illustrated in figure 1. Mechanistically, the reduction of NO_3^- (ads) to nitrite (NO_2^-) (ads) is rate determining. Of the noble (Ru, Rh, Pd, Ir, Pt) and coinage (Cu, Ag, Au) metals, Cu shows the highest activity for NO3RR.[1,3–5] In acidic electrolyte, Cu is the only monometallic electrocatalyst capable of forming nitric oxide (NO) production solution, whereas in alkaline electrolyte NH_3 and NO_2^- primarily form.[4,6,7] All other monometallic noble and coinage metals selectively produce NH_3, hydroxylamine (NH_2OH), and hydrogen.[8] However, no monometallic electrocatalyst is capable of the selective conversion of NO_3^- to benign N_2. Therefore, considerable effort has been devoted to incorporation of a second metal catalyst into the Cu lattice that can selectively convert NO to the environmentally desired N_2 product.

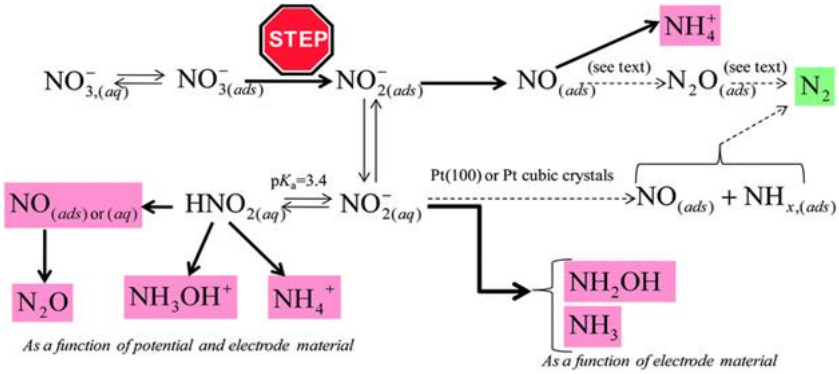

Figure 1. Reaction pathway of the NO_3^- reduction reaction in acidic electrolyte on metallic electrocatalysts.[1] Production of N_2 is environmentally preferential, while conversion of NO_3^- to NH_4^+ has seen increased attention as an alternative to thermal Haber-Bosch.

De Vooys et al. identified N_2O as the precursor to N_2, with N_2O formation only occurring by NO dimerization ($(NO)_2$) when appreciable solution-phase NO (NO_{sol}) is present.[5,9] Of the noble and coinage metals, Pd shows both the highest activity and selectivity for NO reduction to N_2,[9] making it a viable candidate for synergistic NO_3RR to N_2 by alloying with Cu. Indeed, $Cu_{100-x}Pd_x$ catalysts have shown either excellent activity or selectivity for NO_3RR, depending on composition. Electrocatalysts around 80 at% Cu show the highest activity for NO_3RR[10] but poor selectivity to N_2, whereas optimal selectivity for NO_3RR is achieved with >80 at% Pd electrocatalysts, though activity in $Cu_{100-x}Pd_x$ generally worsens with increasing Pd incorporation. This duality makes design of active and selective catalysts challenging for the $Cu_{100-x}Pd_x$ system.[10–12]

Our research focuses on elucidating the activity for NO_3RR of a series of bimetallic $Cu_{100-x}Pd_x$ electrocatalysts in buffered neutral (pH 7) 0.1 M potassium phosphate buffer ($K_xH_{3-x}PO_4$) electrolyte. We seek to better understand the intrinsic kinetics of NO3RR in neutral pH, as kinetics in neutral pH, typical of drinking water used as feedstock, is currently poorly understood. Further, this work offers a first investigation into whether the PO_4^{3-} anion plays an inhibitory role in NO3RR, as has been observed with similar anions found in drinking water (CO_3^{2-}, SO_4^{2-}).[13,14]

Experimental Procedures

All water used was of Milli-Q grade (> 18 MΩ-cm). All electrochemical measurements were performed with EC-Lab software on Biologic VSP-300 or SP-200 potentiostats. Copper-palladium bimetallic catalysts ($Cu_{100-x}Pd_x$) were electrodeposited from aqueous 0.1 M $HClO_4$ (ACS >69.0%) solutions of 10(1-X) $Cu(NO_3)_2$ (Sigma-Aldrich, 99.999%) and 10X $Pd(NO_3)_2$ (Sigma-Aldrich, anhydrous) where X denotes the stoichiometry of Pd in the $Cu_{100-x}Pd_x$ alloys. FTO-coated glass working electrodes (MSE Supplies, TEC 7) were electrically contacted to titanium wires by indium-gallium eutectic (Sigma-Aldrich, ≥ 99.99%) and silver paint (Ted Pella, Leitsilber), and electrically isolated by epoxy (LocTite®, EA 9460). Electrodepositions were carried out in a glass three-electrode cell, with platinum wire counter electrode and a saturated calomel electrode (SCE) reference. The charge passed at the working electrode necessary to develop a film of a given nominal thickness was determined by the relationship 0.01 C/cm^2-nm,[12] with a target catalyst thickness of 10 nm (0.1 C/cm^2 current density). For electrodeposition, surface area was determined from the geometric surface area of the FTO substrate. Electrodeposition solutions were sparged with N_2 gas through porous glass frits and stirred magnetically with a magnetic Teflon stir bar prior to deposition; during the deposition, the solution was blanketed with N_2 without stirring. Cathodic electrodepositions were performed chronoamperometrically at -0.25 V vs SCE, where voltammetry indicates mass-transfer limited electrodeposition for both $Cu(NO_3)_2$ and $Pd(NO_3)_2$ and is before the onset of the hydrogen evolution reaction (HER).[12] Choosing electrodeposition potentials anodic of HER onset ensures that all charge is passed corresponds to the electrodeposition of Pd and Cu. Crystallinity and phase were characterized by X-ray diffraction (XRD; Bruker D8-Discover) and morphology by scanning electron microscopy (SEM; FEI Quanta 600SEM).

Electrocatalytic measurements were performed in a glass three-electrode cell with $Cu_{100-x}Pd_x$ working electrode, Pt wire counter electrode, and Ag/AgCl reference electrode. Cyclic voltammetry measurements were performed in a quiescent, Ar-blanketed aqueous 0.1 M pH 7 potassium phosphate buffer ($K_xH_{3-x}PO_4$) electrolyte with a series of $NaNO_3$ concentrations (0, 1.613, 10, and 100 mM). Chronoamperometric measurements were performed in the same solutions, but with a stir bar rotating at 500 rpm. Solutions were purged with Ar for 30 minutes prior to testing. Potentials were corrected for solution and contact resistance Ohmic losses (iR) by identification from PEIS at 0 V vs open circuit (E_{oc}).[15–17] Electrochemically active surface area (ECSA) was determined by measuring the double layer capacitance response as a function of CV sweep rate (mV/s) in a non-Faradaic region of the CV profile.

Results and Discussion

Cyclic voltammetry (CV) was performed in 0.1 M $K_xH_{3-x}PO_4$ buffer for a series of $Cu_{100-x}Pd_x$ electrodeposited films at a series of $NaNO_3$ concentrations. The CV for the Cu_{100} electrocatalyst in 0 mM $NaNO_3$ (figure 2) indicate a local maximum (0 V_{RHE}) and minimum (-0.13 V_{RHE}), which is indicative of a reversible redox event. Sweeping from positive to negative potentials from 0 V, the initial cathodic peak likely corresponds to the reduction of Sn^{2+} to Sn^0 in the reaction SnO + $2e^-$ → Sn + O^{2-}.[18] This step precedes the hydrogen evolution reaction (HER), or the formation of H_2 from 2 H^+ and 2 e^-; the onset of this reaction occurs around -0.2 V_{RHE} and is evident from the exponential takeoff in current density. The anodic peak at 0 V_{RHE} is likely the concurrent oxidation of Sn^0 back to Sn^{2+}. These redox features are lost in the 100 mM solution, which is due to the additional current from the reduction of NO_3^-. It is assumed that this additional current corresponds to the rate-limiting step of NO_3RR, which is NO_3^- + H_2O + $2e^-$ → NO_2^- + $2OH^-$ and has an onset potential around 0 V_{RHE} on the 100 mM plot.[6,18]

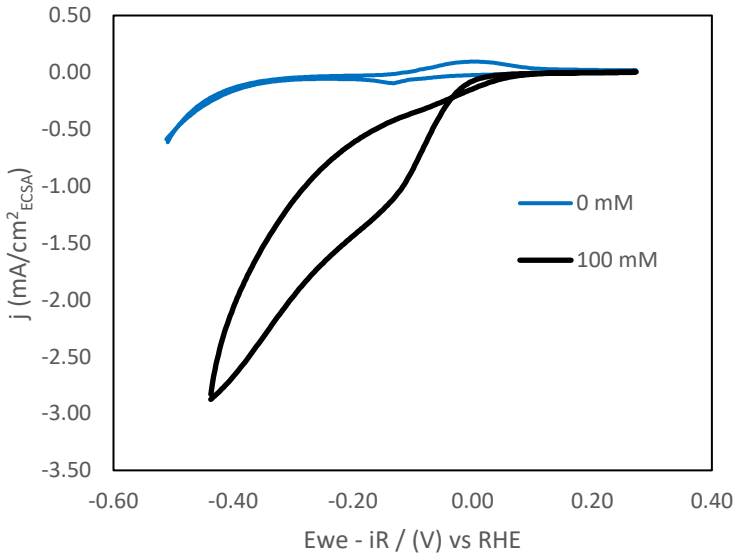

Figure 2. CV of Cu_{100} electrode in 0.1 M $K_xH_{3-x}PO_4$ with 0 mM and 100 mM $NaNO_3$. Potential sweeps were recorded at 10 mV/s at room temperature.

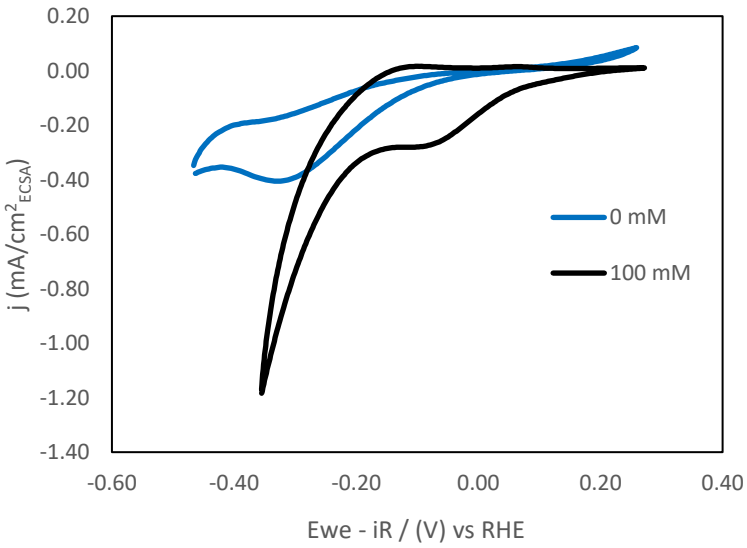

Figure 3. CV of $Cu_{75}Pd_{25}$ electrode in 0.1 M $K_xH_{3-x}PO_4$ with 0 mM and 100 mM $NaNO_3$. Potential sweeps were recorded at 10 mV/s at room temperature.

Voltammograms in figure 3 show the performance of $Cu_{75}Pd_{25}$ under the same conditions. At 0 mM $NaNO_3$, the peak at -0.35 V_{RHE} in the cathodic sweep is likely due to the intercalation of hydrogen in to the Pd lattice to form PdH.[10,11] Pd is known to adsorb hydrogen well while Cu only weakly adsorbs hydrogen, which is why there are no hydride formation features in the Cu_{100} CV.[10] The PdH peak occurs at a more anodic potential in the 100 mM solution, which may be due to adsorbed NO_3^- blocking sites for

hydrogen to active sites on the Cu-Pd alloy. HER onset occurs at -0.15 V_{RHE} at 100 mM $NaNO_3$, and NO_3RR onset occurs at 0.2 V_{RHE}. Additionally, the maximum current density reached by $Cu_{75}Pd_{25}$ is lower than that reached by the Cu_{100} electrocatalyst.

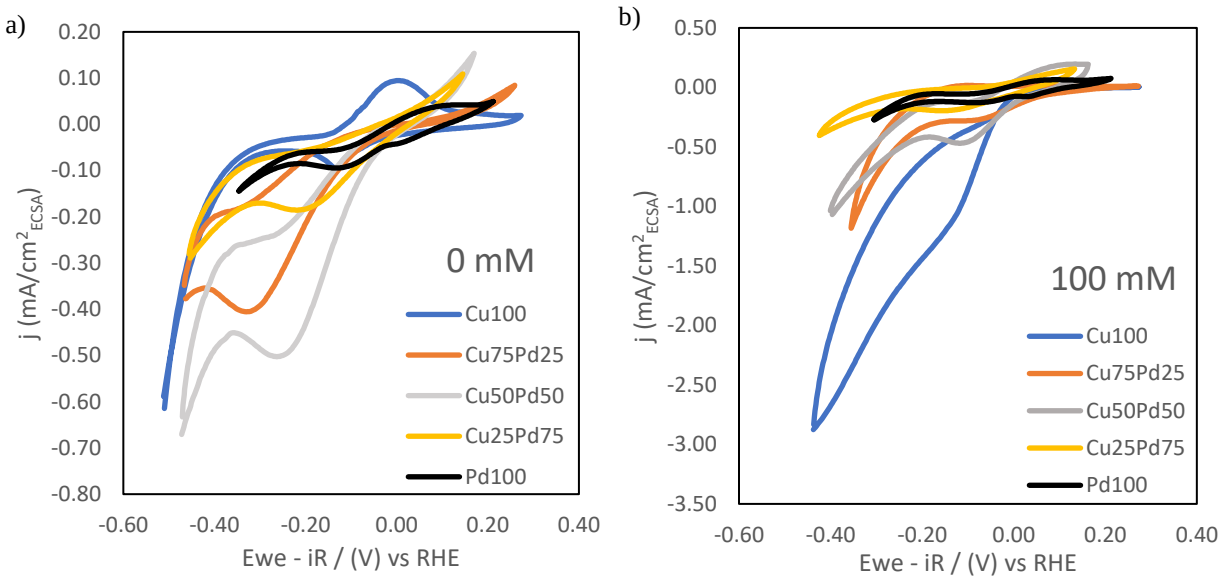

Figure 4. Cyclic voltammograms of $Cu_{100-x}Pd_x$ in 0.1 M $K_xH_{3-x}PO_4$ with a) 0 mM $NaNO_3$ and b) 100 mM $NaNO_3$. Scan rates were run at 10 mV/s. Current density is corrected by the electrodes' ECSA.

Overlaid voltammograms for all $Cu_{100-x}Pd_x$ electrocatalysts at 0 and 100 mM $NaNO_3$ are shown in figure 4. Hydride formation and HER onset potentials shifts to more anodic potentials with increasing Pd incorporation into the Cu lattice. This is indicative of decreased efficiency for NO_3RR and is consistent with findings from Mattarozzi et. al.[12] Additionally, the peak current density achieved for NO_3RR and HER appears to decrease with increasing Pd concentration, where the largest current was produced by the Cu_{100} electrocatalyst. This trend slightly deviates from results found by Anastasopoulos et. al[10], who observed the trend $Cu_{85}Pd_{15}$ > $Cu_{75}Pd_{25}$ > Cu_{100} in NO_3RR activity. It is possible that this difference is due to the variation in surface composition of CuPd phases; Cu is known to segregate from CuPd alloy sites, and so perhaps pure Cu site dominate the surface and negate the improved kinetics from small Pd additions.[10] This can be determined by an in-depth analysis of the surface composition using XRD and SEM techniques.

For an elementary reaction, the order of a reaction is the sum of the stoichiometric ratios of the reactants. In a rate law, it is the sum of the exponents for the reactant concentrations; for instance, a generic rate law can be shown as $r = k[A]^a[B]^b$ from the reaction $aA + bB \rightarrow cC$, where the overall reaction order would be a+b. Thus, the reaction order describes how the rate of the reaction depends on the concentration of the reactants. Figure 5 shows the reaction order with respect to NO_3^- for the $Cu_{100-x}Pd_x$ electrocatalysts at potentials in the NO_3RR range. Electrocatalysts with >50 at% Pd have 0^{th} order characteristics over all potentials, which means that, for these compositions, the rate of NO_3RR is relatively independent of reactant concentration. However, the Cu_{100} electrocatalyst attains a maximum reaction order of 0.93 around -0.25 V_{RHE}, and the $Cu_{75}Pd_{25}$ electrocatalyst attains a maximum reaction order of 0.55 around 0 V_{RHE}. This implies that

electrocatalysts with >75 at% Cu are at least partially dependent on the concentration of NO_3^- in solution.

Tafel analysis is a mathematical analytic method that provides insight into the mechanism of an electrocatalytic process, such as redox events and irreversible electrochemical reactions. It is partly derived from the Butler-Volmer equation, which describes an exponential increase in the rate of a redox reaction as a function of the applied potential in an electrochemical system. For a single electron transfer reaction, such as the rate limiting step in NO_3RR ($NO_3^- + e^- \rightarrow NO_2^-$), there is a linear relationship between the applied potential at the working electrode and the logarithmic current density measured. A line of best fit can be obtained, and the slope of the linear region extracted. This model assumes that the flux of charged species is uniform across the electrode surface and the concentration of species at the interface is equal to the bulk concentration.[19] Curved regions of the Tafel plots are indicative of mass transfer limitations of chemical species to the electrode surface, a change in reaction mechanism, or change in selectivity when multiple reactants compete for charge passed. In measurement of NO_3RR at high NO_3^- concentration, curved regions likely correspond to the transition between kinetic and mass transport limited rate of reaction.

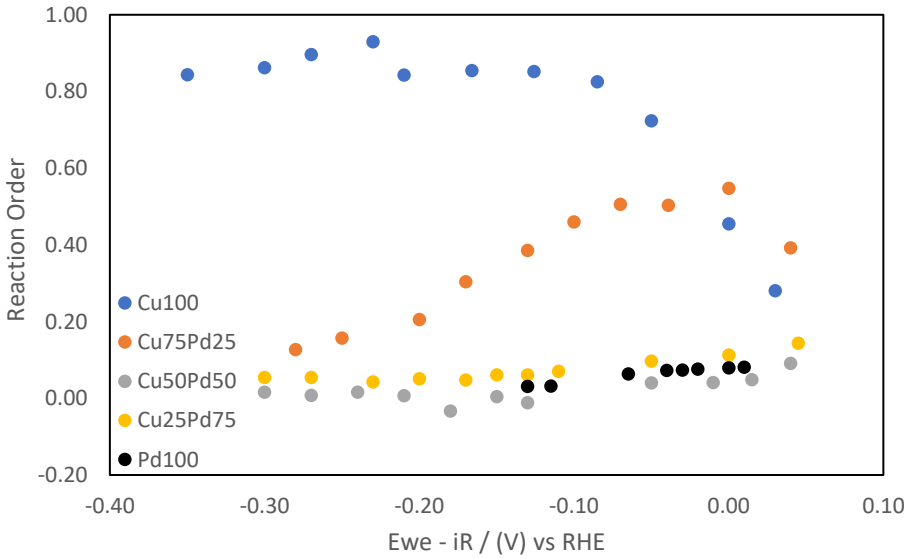

Figure 5. Reaction rate order of $Cu_{100-x}Pd_x$ electrocatalysts as a function of applied potential. Values were derived from measurements taken from chronoamperometry experiment.

Tafel plots for the $Cu_{100-x}Pd_x$ electrocatalysts in 0 and 100 mM $NaNO_3$ solutions are shown in figure 6. Linear regression equations were obtained over the potential range associated with the rate-limiting step of NO_3RR. For these plots, the slopes of the linear regions are correlated to the transfer coefficient of the redox reaction; slopes that are closer to 0 indicate more efficient electron transfer kinetics for this specific reaction. Comparing the values of the slopes between the 0 mM $NaNO_3$ (HER) and 100 mM $NaNO_3$ (NO_3RR) solutions, there is a general decrease in the absolute value of the slopes for all electrocatalyst compositions when $NaNO_3$ is introduced. Comparing compositions, the slope values generally decrease with increased Cu at%, which indicates that the efficiency of the reaction is proportional to Cu at% in the electrocatalysts. This trend is expected since Cu is known to have high activity for the conversion of NO_3^- to NO_2^- and an increase in Pd at% in $Cu_{100-x}Pd_x$ electrocatalysts has been correlated to a decrease in activity.[10,12] Although these plots and their corresponding linear regions provide good insight, the actual mechanism of the reaction is still unclear. Without quantifying the species produced by this reaction, it is unknown

whether the $NO_3^- + e^- \rightarrow NO_2^-$ reaction is indeed the rate-limiting step or another nitrogen

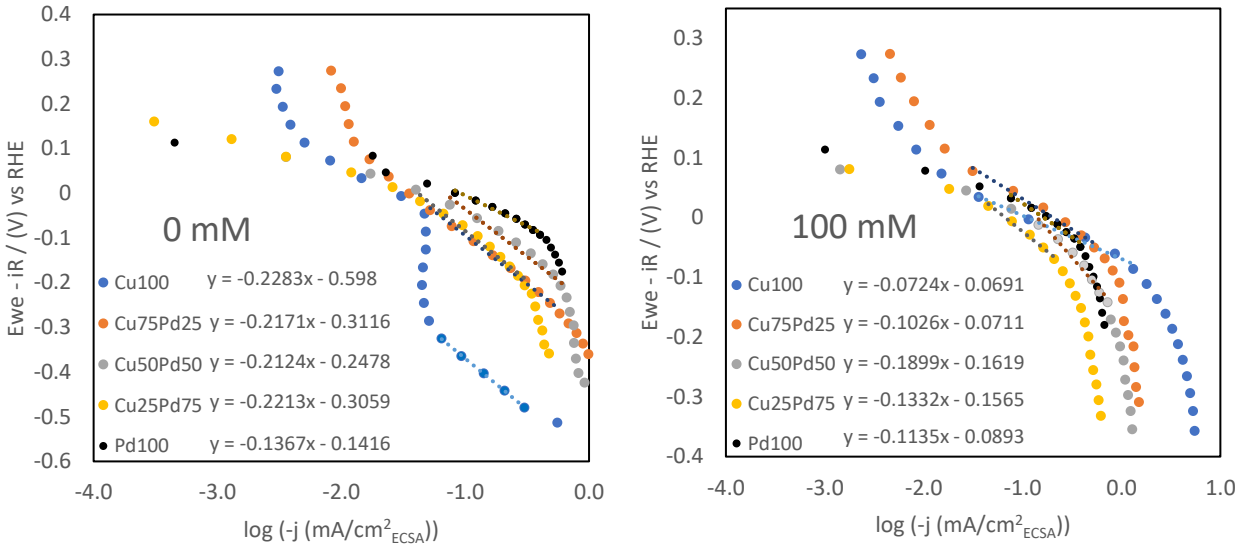

Figure 6. Tafel plots of $Cu_{100-x}Pd_x$ electrocatalysts in 0.1 M $K_xH_{3-x}PO_4$ with 0 and 100 mM $NaNO_3$.

redox reaction, or a combination of the two. Additionally, the applied potential range used to derive the linear regression equations needed to be smaller for the 100 mM NO_3^- to ensure a relatively high R^2 value; this indicates that reaction is affected by the mass transfer of NO_3^- to the electrode surface. This effect is most pronounced in the electrocatalysts with high Pd content, potentially because the surfaces of these catalysts have non-uniform compositions of Cu, Pd, and Cu-Pd alloy active sites. These sites will adsorb NO_3^- and catalyze the reduction at different rates, and so the overall kinetics will not be as uniform as the more homogenous electrocatalysts like Cu_{100}.

Conclusion

In conclusion, five $Cu_{100-x}Pd_x$ electrocatalysts (estimated thicknesses of 50 nm) were electrodeposited on FTO substrates. These electrodes were tested electrochemically in neutral pH solutions composed of 0.1 M $K_xH_{3-x}PO_4$ and varying amounts of $NaNO_3$. Cyclic voltammograms show that the pure Cu electrode displays the highest activity for NO_3RR. Increasing Pd at% in the electrocatalysts resulted in a general decrease in activity for NO_3RR, as previously reported in other studies with bimetallic Cu-Pd alloys. Chronoamperometry was used to obtain reaction order for a range of applied potential and for Tafel analysis. The Cu_{100} and $Cu_{75}Pd_{25}$ electrocatalysts show at least partial 1st order kinetics, while the remaining electrocatalysts follow 0th order kinetics over NO_3RR potentials. Tafel plots show Cu_{100} has the most efficient transfer coefficient for NO_3RR, and that increased Pd incorporation into the Cu matrix is correlated with a loss of efficiency.

For future experimentation, the next logical step is to identify and quantify nitrogen species that are produced during NO_3RR. This would help clarify what reactions are catalyzed by each electrocatalyst and determine their selectivity towards the desirable N_2 product. It would also be valuable to synthesize electrocatalysts with lower thicknesses (<10 nm) which would promote better electron transfer across the catalyst-FTO interface. In

addition, electrochemical tests could be performed using a rotating disk electrode (RDE), which would ensure uniform mass transfer over the surface of the electrode.

Acknowledgments

Additional support of summer research was provided by the Pete and Rosalie Johnson Undergraduate Internship Program and OSU Clean Water Initiative. Supplies were provided by OSU startup funds and the Callahan Faculty Scholar funds. A portion of the research was performed using EMSL (grid.436923.9), a DOE Office of Science User Facility sponsored by the Biological and Environmental Research program. A special thanks to Kelsey Stoerzinger and Quinn Carvahlo for guiding and facilitating the honors thesis process.

References

1. M. Duca and M. T. M. Koper, *Energy Environ. Sci.*, **5**, 9726–9742 (2012).
2. K. Wick, C. Heumesser, and E. Schmid, *J. Environ. Manage.*, **111**, 178–186 (2012).
3. J. X. Liu, D. Richards, N. Singh, and B. R. Goldsmith, *ACS Catal.*, **9**, 7052–7064 (2019).
4. A. C. A. De Vooys, R. A. Van Santen, and J. A. R. Van Veen, 27–42 (2000).
5. G. E. Dima, A. C. A. De Vooys, and M. T. M. Koper, *J. Electroanal. Chem.*, **554**–**555**, 15–23 (2003).
6. D. Reyter, D. Bélanger, and L. Roué, *Electrochim. Acta*, **53**, 5977–5984 (2008).
7. S. E. Bae, K. L. Stewart, and A. A. Gewirth, *J. Am. Chem. Soc.*, **129**, 10171–10180 (2007).
8. G. E. Dima, G. L. Beltramo, and M. T. M. Koper, *Electrochim. Acta*, **50**, 4318–4326 (2005).
9. A. C. A. De Vooys, M. T. M. Koper, R. A. Van Santen, and J. A. R. Van Veen, *J. Catal.*, **202**, 387–394 (2001).
10. A. Anastasopoulos, L. Hannah, and B. E. Hayden, *J. Catal.*, **305**, 27–35 (2013) http://dx.doi.org/10.1016/j.jcat.2013.04.010.
11. D. Reyter, D. Bélanger, and L. Roué, *J. Phys. Chem. C*, **113**, 290–297 (2009).
12. L. Mattarozzi et al., *Electrochim. Acta*, **230**, 365–372 (2017).
13. Y. Wang, J. Qu, and H. Liu, *J. Mol. Catal. A Chem.*, **272**, 31–37 (2007).
14. S. Bae, J. Jung, and W. Lee, *Chem. Eng. J.*, **232**, 327–337 (2013) http://dx.doi.org/10.1016/j.cej.2013.07.099.
15. C. Wei et al., *Adv. Mater.*, **31**, 1–24 (2019).
16. D. Van Der Vliet et al., *J. Electroanal. Chem.*, **666**, 89 (2012) http://dx.doi.org/10.1016/j.jelechem.2011.12.008.
17. D. M. Morales and M. Risch, *J. Phys. Energy* (2021).
18. M. S. Antelman and F. J. Harris, *Encycl. Chem. Electrode Potentials*, 1–81 (1982).
19. D. Li, C. Lin, C. Batchelor-McAuley, L. Chen, and R. G. Compton, *J. Electroanal. Chem.*, **826**, 117–124 (2018).

Supplemental Information

a. Cyclic Voltammograms

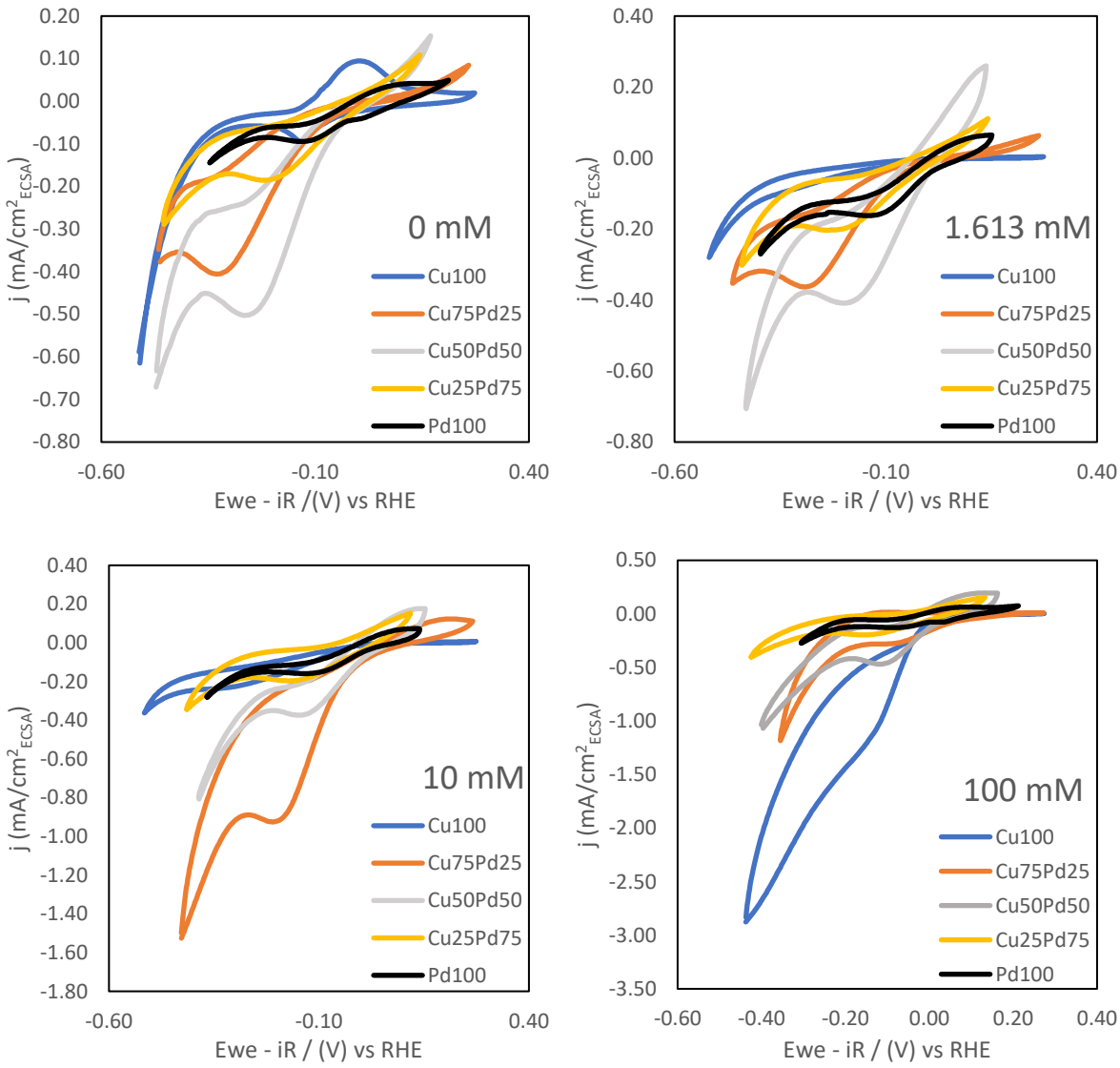

Figure 7. Cyclic voltammograms of $Cu_{100-x}Pd_x$ in 0.1 M $K_xH_{3-x}PO_4$ with 0, 1.613, 10 and 100 mM $NaNO_3$.

b. Tafel Plots

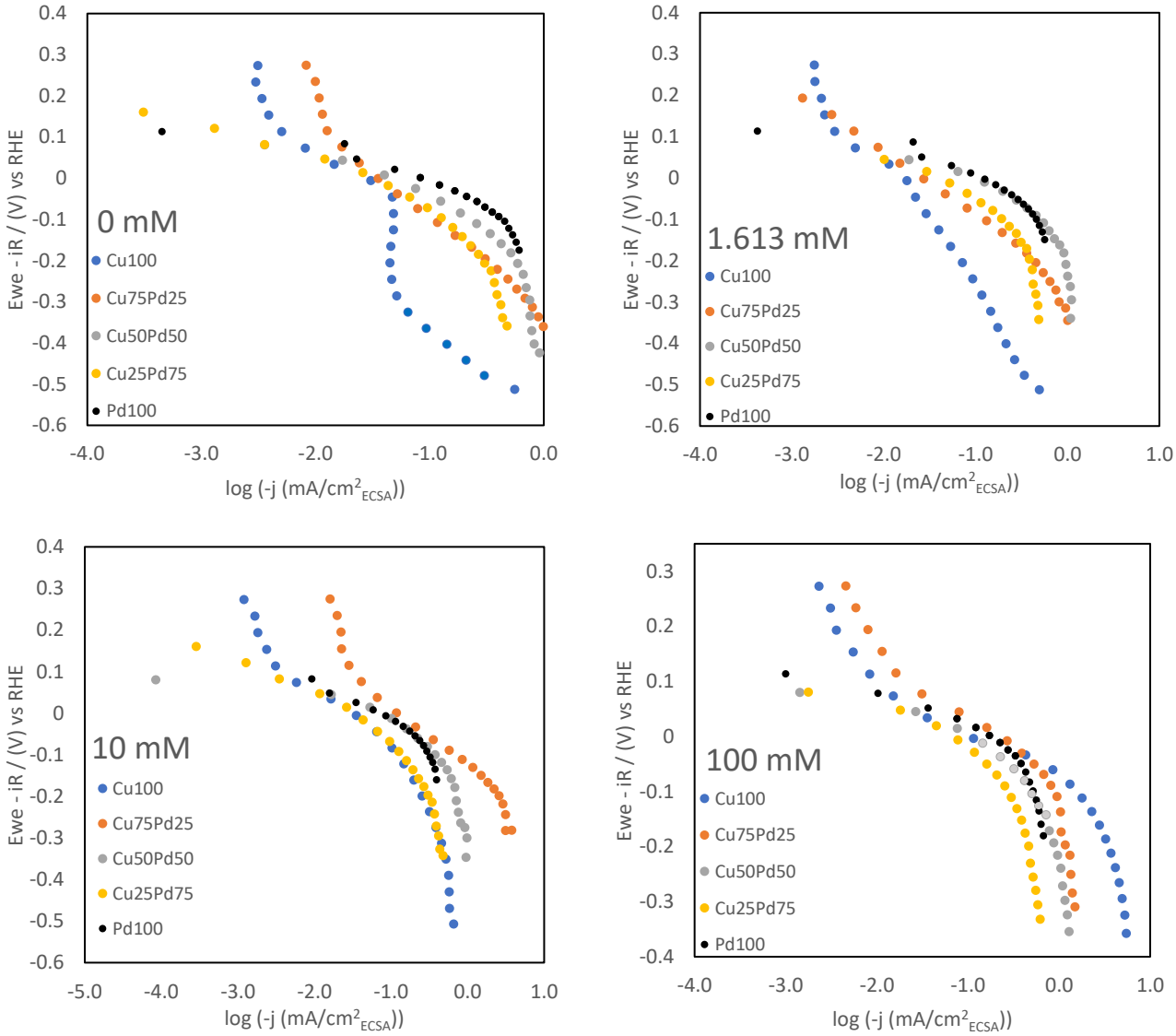

Figure 8. Tafel plots of $Cu_{100-x}Pd_x$ electrocatalysts in 0.1 M $K_xH_{3-x}PO_4$ with 0, 1.613, 10 and 100 mM $NaNO_3$.